(Received 12 April 2024, Accepted 10 May 2024, Scheduled 22 May 2024)

Optically Transparent Broadband Microwave Absorber with Tunable Absorptivity Based on Graphene-ITO Structure

Shuomin Zhong[1, 2, 3, *], Enbang Yu[3], Yu Zhang[3], Xianjia Chen[3], Zi-Wei Zheng[4], Qiping Lin[2], and Sailing He[1]

[1] *State Key Laboratory of Modern Optical Instrumentations Centre for Optical and Electromagnetic Research, Zhejiang University, Hangzhou 310058, China*
[2] *Qijing Machinery Co., LTD, Ninghai 315600, China*
[3] *School of Information Science and Engineering, Ningbo University, Ningbo 315211, China*
[4] *Digital Industry Research Institute, Zhejiang Wanli University, Ningbo 315211, China*

ABSTRACT: In this study, we present a novel broadband microwave absorber that is both optically transparent and capable of dynamically adjusting its absorptivity. The absorber is composed of a graphene sandwich structure (GSS), a polyvinyl chloride (PVC) layer, an indium tin oxide (ITO) layer, another PVC layer, and an ITO ground plane, arranged in a top-to-bottom configuration. This unique design allows for a working bandwidth of 6.8 GHz to 14.0 GHz, with absorption levels ranging from 95% to 60%, achieved by varying the impedance of the GSS from 1000 Ω/sq to 200 Ω/sq through tuning the bias voltage. By utilizing materials with high optical transmittance, this nonpatterned device maintains exceptional optical transparency. Furthermore, by incorporating additional ITO layers with different impedances at equal intervals, this multilayer design can be extended to create an ultra-broadband absorber covering a range of 5.28–39.52 GHz. This is made possible due to the dispersionless resistance of nonpatterned graphene and ITO sheets in the microwave spectrum. This transparent wideband microwave absorber, with tunable absorptivity, holds great potential for a wide range of applications in broadband and intelligent stealth technology.

1. INTRODUCTION

Microwave absorbers (MAs) have been widely studied over the past several decades, for circumventing electromagnetic (EM) interference [1] and pollution [2] caused by undesirable EM waves, or reducing radar cross section in stealth applications [3]. Compared with conventional absorbers, metamaterial absorbers have great advantage in realizing tunable absorption responses, with a larger scope of applications. By constructing metamaterials using new materials such as graphene, vanadium dioxide, and ITO, many absorbers with special functions can be realized. For instance, optically transparent MAs which are highly demanded in windows of buildings and aircrafts can be designed using transparent ITO material [4–6], which is unrealizable using carbon [7], ferrite [8], or circuit analog absorbers [9] due to their optical opacity.

ITO is a transparent film with dispersionless surface resistance across microwave bands and can be used as resistive layers in microwave absorbers [10–12]. Similarly, graphene can also be modeled as a resistive sheet with impedance of $R_g + jX_g$. In microwave bands, the impedance of graphene is also dispersionless and dependent on the carrier concentration related to the Fermi level [13, 14]. By integrating two graphene sheets and an electrolyte medium between them to form graphene sandwich structure (GSS), the impedance in the whole microwave band can be tuned through varying biasing voltages [15]. Many reconfigurable graphene absorbers including frequency-tunable [16–19], angle-tunable [20], amplitude-tunable [21–23], and bandwidth-tunable [24] absorbers have been proposed experimentally by using various GSS-metamaterial hybrid structures. However, most of them are not optically transparent due to the use of opaque metal structures and tunable devices. In [19], by utilizing transparent ITO, graphene, and PVC substrates, an optically transparent absorber with tunable frequency has been realized. Nevertheless, its high-absorptivity bandwidth is narrow since the impedance of patterned graphene and ITO is frequency-dependent [25]. Therefore, an amplitude-tunable microwave absorber with both high optical transparency and broad operating bandwidth is still not reported.

In this study, we have utilized the exceptional properties of ITO and graphene in terms of transparency and dispersionless impedance in microwaves, to create a transparent MA that possesses both amplitude-tunable broadband microwave absorption and high optical transparency. To achieve this, we employed a GSS-PVC-ITO-PVC-ITO hybrid structure. By increasing the number of ITO layers with different sheet resistances (which are commercially available and can be ordered accordingly), the bandwidth of absorption $> 90\%$ can be broadened by 152.8%, achieving a range from 5.28 GHz to 39.52 GHz, which is a significant improvement in the absorption capabilities of the MA. By altering the bias voltage across the GSS on the top for impedance tuning of graphene from 1000 Ω/sq to 200 Ω/sq, the reflectivity of the whole MA can be

* Corresponding author: Shuomin Zhong (zhongshuomin@nbu.edu.cn).

modulated from -13.4 dB to -3.8 dB across an extremely wide operational band. To validate our idea, we fabricated a prototype using the GSS-PVC-ITO-PVC-ITO configuration. The experimental outcomes verified that the absorptivity of this design could be adjusted from 95% to 60% by applying a bias voltage ranging from 0 V to 5 V to the GSS. This adaptable absorber design maintains exceptional optical transparency due to the see-through properties of all the materials utilized in its assembly.

2. DESIGN OF THE TRANSPARENT ABSORPTIVITY-TUNABLE ABSORBER

Figure 1 illustrates the composition of this design, which consists of five distinct parts arranged from top to bottom. These parts include the GSS positioned at the top, followed by the middle ITO layer with a sheet resistance of $R_{i1} = 120\,\Omega$/sq. The ITO layer with a sheet resistance of $R_{i2} = 6\,\Omega$/sq is located at the bottom, and two PVC dielectric spacers with a thickness of $H = 4$ mm are positioned between these layers. All the GSS and ITO layers are non-patterned films that are attached to polyethylene terephthalate (PET) substrates with a thickness of 0.125 mm. The permittivities for PET and PVC are $2.8 + 0.056i$ and $3 + 0.06i$, respectively. The GSS is composed of two graphene layers and a diaphragm paper with a thickness of 50 μm, which is soaked with 1-Butyl-3-methylimidazolium hexafluorophosphate ([BMIM] PF6) ionic liquid. By applying a bias voltage across the GSS, as depicted in Fig. 1(c), the Fermi level of graphene can be adjusted by controlling the voltage U. Consequently, this adjustment enables the tunability of the surface impedance of graphene within the microwave frequency range.

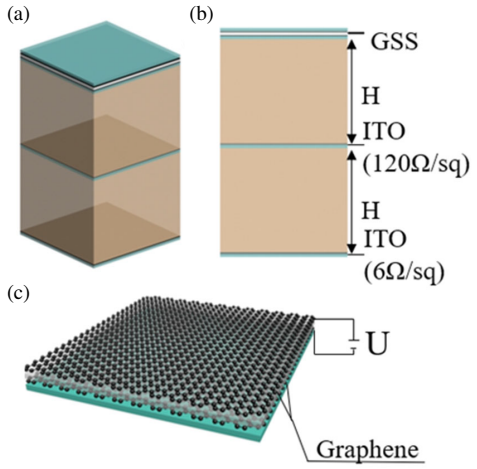

FIGURE 1. (a) Overall structure. (b) Side view. (c) Schematic of the GSS.

2.1. Equivalent Circuit Model and Simulations

In microwave bands, the surface conductivity of graphene can be simplified as denoted by [14]

$$\sigma_g = -j\,\frac{e^2 E_F}{\pi\hbar^2\,(\omega - j\gamma)}, \tag{1}$$

where e is the electron charge, E_F the Fermi level, $\hbar$ is Planck's constant, and γ the scattering rate of electrons. The impedance of the graphene layer, denoted as $Z_g = 1/\sigma_g$, can be expressed as a complex function $Z_g = R_g + jX_g$. In the scenario where the frequency ω is significantly smaller than the scattering rate γ (with a value of 3.92×10^{12} Hz in this case), the inductance X_g can be negligible due to its significantly smaller value than R_g ($X_g \ll R_g$). Consequently, the monolayer graphene can be effectively modeled as a purely resistive sheet with dispersionless sheet resistance in the whole microwave bands, in agreement with previous literature [15–24].

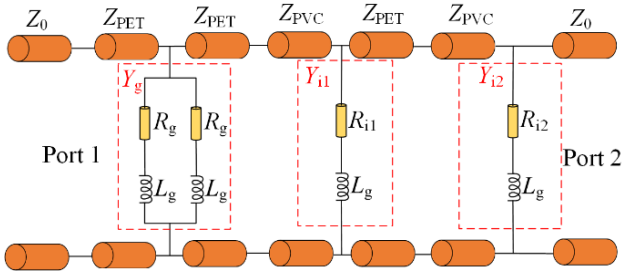

FIGURE 2. The equivalent circuit model of the absorptivity-tunable absorber. $Y_g = 2/R_g$, $Y_{i1} = 1/R_{i1}$, $Y_{i2} = 1/R_{i2}$.

The design and optimization of the absorber are guided by an equivalent circuit model (ECM), as depicted in Fig. 2. The graphene and ITO sheets are represented by resistance values R_g, R_{i1}, and R_{i2}, respectively. The inductance L_g can be negligible within the microwave frequency range of interest. The GSS can be represented as two resistors R_g in parallel. The diaphragm paper is also neglected in the ECM due to its negligible thickness compared to the operating wavelength. The PET and PVC substrates are modeled as sections of a transmission line, with lengths of $t_1 = 0.125$ mm and $t_2 = H = 4$ mm, respectively. The characteristic impedances of these substrates are given by $Z_{\text{PET}} = Z_0/\sqrt{\varepsilon_{\text{PET}}}$ and $Z_{\text{PVC}} = Z_0/\sqrt{\varepsilon_{\text{PVC}}}$, respectively, where Z_0 represents the characteristic impedance. The entire structure can be described as a two-port network, and its transmission ($ABCD$) matrix can be obtained as

$$\begin{aligned}
&\begin{bmatrix} A & B \\ C & D \end{bmatrix} = \begin{bmatrix} \cos\beta_1 t_1 & jZ_{\text{PET}}\sin\beta_1 t_1 \\ j\,\frac{1}{Z_{\text{PET}}}\sin\beta_1 t_1 & \cos\beta_1 t_1 \end{bmatrix} \\
&\begin{bmatrix} 1 & 0 \\ Y_g & 1 \end{bmatrix} \begin{bmatrix} \cos\beta_1 t_1 & jZ_{\text{PET}}\sin\beta_1 t_1 \\ j\,\frac{1}{Z_{\text{PET}}}\sin\beta_1 t_1 & \cos\beta_1 t_1 \end{bmatrix} \\
&\begin{bmatrix} \cos\beta_2 t_2 & jZ_{\text{PVC}}\sin\beta_2 t_2 \\ j\,\frac{1}{Z_{\text{PVC}}}\sin\beta_2 t_2 & \cos\beta_2 t_2 \end{bmatrix} \begin{bmatrix} 1 & 0 \\ Y_{i1} & 1 \end{bmatrix} \\
&\begin{bmatrix} \cos\beta_1 t_1 & jZ_{\text{PET}}\sin\beta_1 t_1 \\ j\,\frac{1}{Z_{\text{PET}}}\sin\beta_1 t_1 & \cos\beta_1 t_1 \end{bmatrix} \\
&\begin{bmatrix} \cos\beta_2 t_2 & jZ_{\text{PVC}}\sin\beta_2 t_2 \\ j\,\frac{1}{Z_{\text{PVC}}}\sin\beta_2 t_2 & \cos\beta_2 t_2 \end{bmatrix} \begin{bmatrix} 1 & 0 \\ Y_{i2} & 1 \end{bmatrix},
\end{aligned} \tag{2}$$

where β_1 and t_1 are the propagation constant and thickness of PET; β_2 and t_2 are the propagation constant and thickness

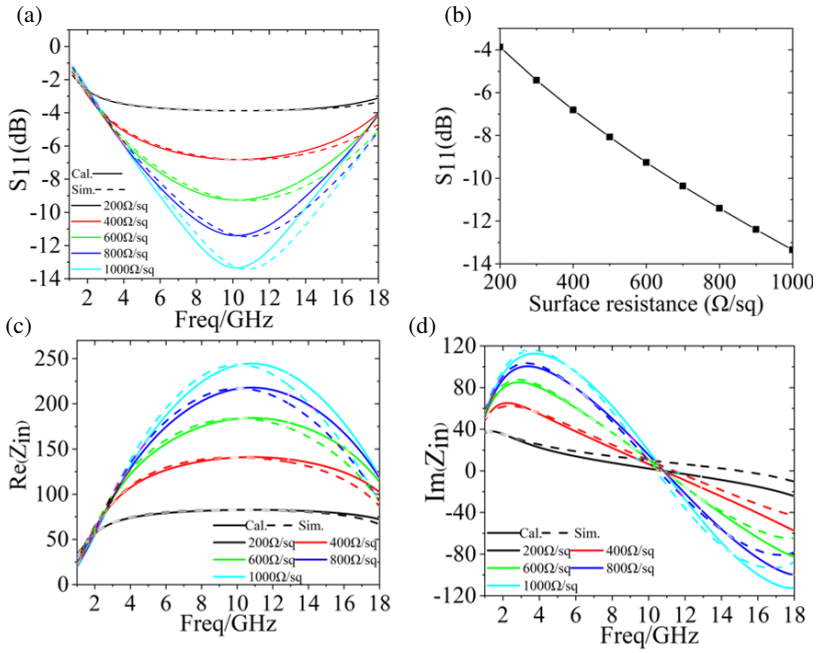

FIGURE 3. The calculated and simulated (a) reflection coefficient and (b) the variation of S_{11} at 10 GHz when the surface resistance of graphene changes. The (c) real and (d) imaginary parts of the input impedance of the tunable absorber. The sheet impedance of graphene varies from 200 to 1000 Ω/sq.

of PVC, respectively. By utilizing the conversion between $ABCD$ and S parameters [26], the reflection and transmission coefficients, S_{11} and S_{21} can be determined. In this case, the transmission coefficient S_{21} is below -30 dB due to the effective shielding effect of the ITO ground plane, which has a low surface resistance of 6 Ω/sq. Consequently, the absorption can be approximated as $A = 1 - |S_{11}|^2$.

The reflection coefficient S_{11} is determined through the ECM and simulated using a full-wave simulation technique. In Fig. 3(a), the S_{11} values obtained from simulations are represented by dotted lines, while the S_{11} values from the ECM are shown by solid lines. The S_{11} curve reaches its minimum at 10 GHz, and the depth of the S_{11} dip can be dynamically altered from -13.34 dB to -3.8 dB, corresponding to a change in absorptivity from 95% to 60%, as the impedance of graphene varies from 1000 Ω/sq to 200 Ω/sq. The simulated outcomes exhibit a strong correlation with those of the ECM, validating the model. When R_g equals the maximum available value of 1000 Ω/sq, the S_{11} at 10 GHz is at its lowest point of -13.8 dB. Furthermore, S_{11} remains below -10 dB from 6.8 GHz to 14.0 GHz (absorptivity $>$ 90%), with a fractional bandwidth of 69.2%. As R_g decreases to the minimum value of 200 Ω/sq, the S_{11} at 10 GHz rises to -3.8 dB. As depicted in Fig. 3(b), the reflectivity at 10 GHz and the surface resistance of graphene R_g exhibit a monotonically decreasing relationship.

The physical insight of the amplitude-tunable absorber is further explored by analyzing the input impedance Z_{in}, calculated using $Z_{in} = Z_0(1 + S_{11})/(1 - S_{11})$. In Figs. 3(c) and 3(d), the imaginary part of Z_{in} is zero at 10 GHz, while the real part ranges from 243.6 Ω to 83 Ω with changing graphene impedance. Due to the nonpatterned graphene with dispersionless impedance, the operating frequency with peak absorption is stable during the tuning process. In contrast, Ref. [16] presents a patterned graphene metasurface with wide absorption band. However, varying GSS resistance causes the absorption curves of the patterned design to split into two peaks, impacting tunable performance in broad band.

2.2. Extending Bandwidth by Introducing More ITO Layer

The GSS-ITO multilayer design plays a crucial role in expanding the absorption bandwidth. Here, we conducted a numerical analysis to evaluate the absorption performance when an additional ITO layer is incorporated into the design, along with air spacers placed between the ITO and GSS layers. Fig. 4(a) illustrates the thickness of air layers, which is set at $L = 3$ mm, while the surface impedance of the three ITO layers varies from 600 Ω/sq, 250 Ω/sq, to 5 Ω/sq from top to bottom. The reflection coefficient S_{11} of this absorber is presented in Fig. 4(b), demonstrating an absorption rate exceeding 90% across the frequency range of 5.28–39.52 GHz. This absorption range corresponds to a fractional bandwidth of 152.8%. The amplitude of reflection can be adjusted from -13 dB to -3.8 dB by varying the graphene impedance from 1000 Ω/sq to 200 Ω/sq. Remarkably, this tuning process maintains a flat response throughout an ultrabroad band.

The input impedance Z_{in} of the absorber is illustrated in Figs. 4(c) and 4(d). The real components of Z_{in} range from 250 Ω to 75 Ω as the R_g varies from 1000 Ω/sq to 200 Ω/sq, while the imaginary component is nearly zero in an ultrabroad absorption band. The addition of a layer with a median impedance value can reduce the dispersion of the imaginary

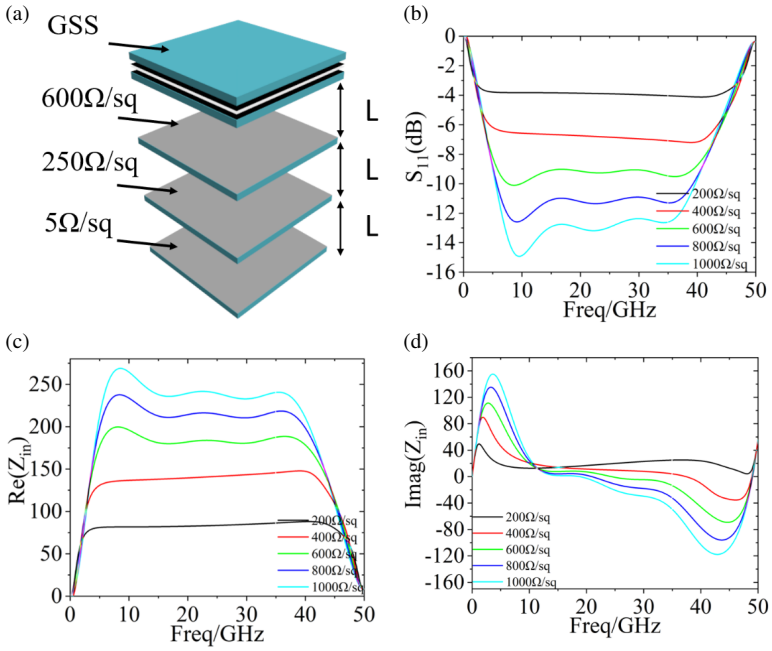

FIGURE 4. (a) GSS-ITO stacked structure with three ITO layers. (b) S_{11} of the absorbers. The (c) real and (d) imaginary parts of the input impedance. The impedance of graphene varies from 200 to 1000 Ω/sq.

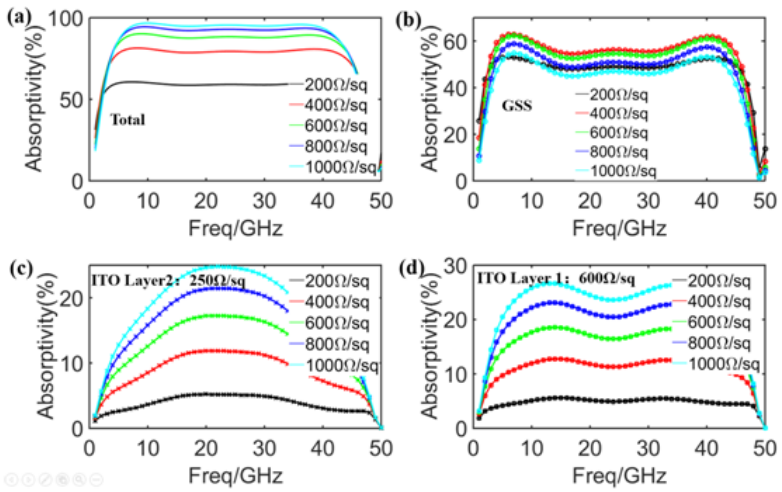

FIGURE 5. Absorptivity (a) of the total absorber, (b) contributed by the GSS, (c) contributed by the 250 Ω/sq-ITO-layer, and (d) contributed by the 600 Ω/sq-ITO-layer, when the graphene impedance varies from 200 to 1000 Ω/sq.

part of impedance across a wide band, aligning the absorber with the air impedance, as depicted in Fig. 4(d), resulting in significantly broad absorption bandwidth. The contribution of each resistive layer to the total absorptivity is also analyzed through simulations, as depicted in Fig. 5. When the graphene impedance varies from 200 to 1000 Ω/sq, the absorptivity contributed by the GSS structure is tuned between 46% and 60%. As shown in Figs. 5(c) and 5(d), the absorptivity contributed by the two ITO layers (i.e., the power losses in the two ITO layers) varies from 5% to 25% when the graphene impedance varies from 200 to 1000 Ω/sq. As the graphene impedance rises from 200 to 1000 Ω/sq, the power passing through the upper GSS during the initial incidence also increases and propagates to the ITO layers, leading to an increase in power loss through the two ITO layers.

3. FABRICATION AND CHARACTERIZATION

To assess the practicality of the proposed amplitude-tunable absorber in Fig. 1, a transparent absorber was created and subjected to experimental testing. The graphene/PET sheets used in the fabrication process were purchased from Ningbo Soft Carbon Electronic Science and Technology Co., Ltd. To verify the relationship between the surface impedance of the graphene and the biasing voltage, a setup similar to the one described in [19] was employed.

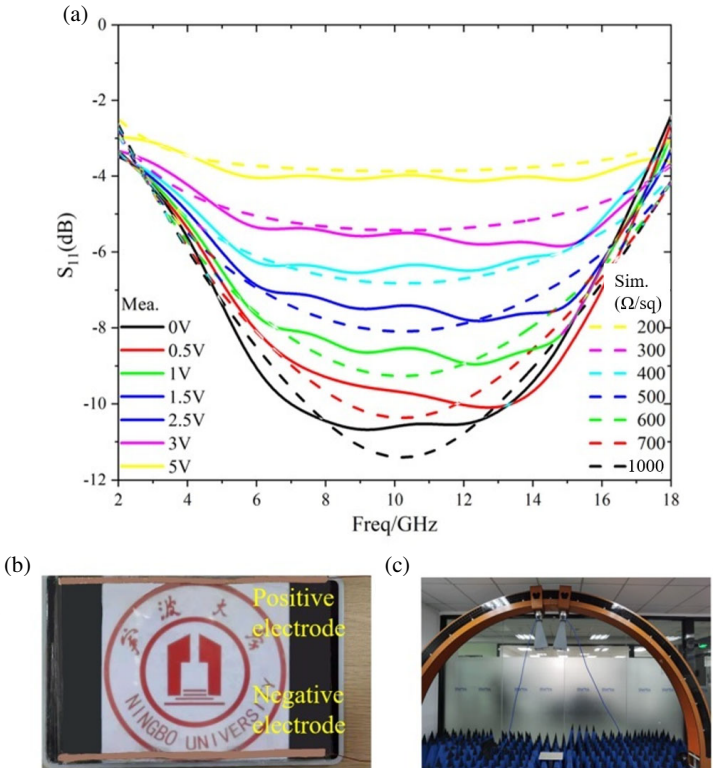

FIGURE 6. (a) Measured and simulated reflection coefficients S_{11} under normal incidence. (b) The prototype. (c) The setup for the test.

During the experiment, the impedance of the graphene ranged from 200 Ω/sq to 1000 Ω/sq. The different layers were adhered together using a 1-μm-thick optical clear adhesive (OCA) known for its exceptional transparency. Two copper electrodes were affixed to the upper and lower graphene sheets to allow for applying bias voltage. The reflections under normal incidence are measured and compared with the simulated ones, as shown in Fig. 6(a). The magnitude of S_{11} was dynamically adjusted from -11.5 dB to -3.6 dB as the bias voltage ranged from 0 V to 5 V. The measurement results have good agreement with the simulations. As depicted in Fig. 6(b), a logo paper placed beneath the prototype remained clearly visible. This transparency is achieved due to the use of transparent and nonpatterned materials in the sample. The light transmittance of the absorber can be estimated by multiplying the transmittance of each layer, which reaches 52%. Two double-ridged horn antennas, connected to the vector network analyzer, were employed for transmitting and receiving the reflected EM signal, as illustrated in Fig. 6(c). The sample was positioned at the center of the arc bridge, which was located 2 meters away from the antennas. To approximate normal incidence, an incidence angle of 5° was used. Additionally, a time gating method was implemented to filter out unwanted scatterings and minimize noise interference. For normalization purposes, a copper plate with the same dimensions as the absorber was measured.

By relocating the antennas, the reflections at various incidence angles for both TE and TM modes were also measured. In Fig. 7(a), it can be observed that the reflection at a 30° incidence angle for the TE mode rises to -10 dB when the graphene has an impedance of 1000 Ω/sq, in contrast to the value at normal incidence. For the TM mode, the reflectivity for oblique incidence is lower than that for normal incidence, decreasing from -11.5 dB (normal incidence) to -13 dB (30° incidence) and -16 dB (45° incidence) when the biasing voltage is 0 V. Nevertheless, as depicted in Fig. 7, the amplitude of absorption for different incident angles (30°, 45°) and both modes could be dynamically regulated with a depth exceeding 5 dB across a broad frequency range when the applied bias voltage was adjusted from 0 V to 5 V. Some minor inconsistencies in the amplitude and bandwidth between the simulation and experimental outcomes are observed, which could be attributed to imperfections in the prototype stemming from the fabrication of GSS and the assembly of the multilayer structure.

Table 1 presents a comparison between various tunable absorbers published in literature and our two designs. The majority of the previous tunable metamaterial absorbers (MAs) are either frequency-tunable [18, 19] or bandwidth-switchable [16, 24]. These tunabilities were achieved through the use of patterned graphene or metal designs, which result in a dispersive impedance of the absorptive or reflective layers, thereby limiting the achieved responses to only frequency manipulation. In [23], amplitude manipulation is achieved; however, the bandwidth is restricted to a mere 18.3%, and the structure lacks transparency. In contrast, our two designs offer optical transparency and absorptivity tunability over an ultra-broadband range (69.2% for the 1# design and 152.8% for the 2# design), while maintaining a moderate thickness.

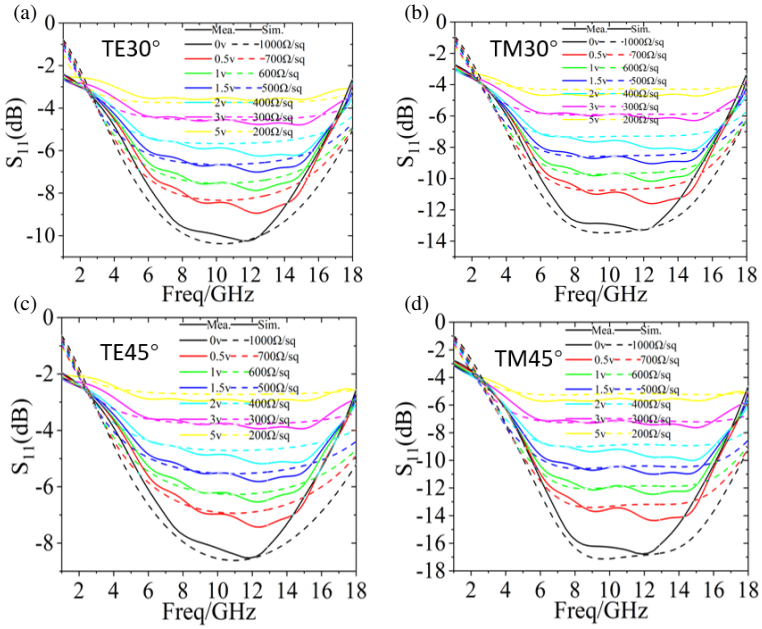

FIGURE 7. The results of S_{11} for (a) 30° and (c) 45° angles under TE mode incidence. The results of S_{11} for (b) 30° and (d) 45° angles under TM mode incidence.

TABLE 1. Comparisons with other referenced broadband absorbers.

Ref.		Working band (GHz)	Absorption relative bandwidth	Relative Thickness (normalized by λ_L)[1]\ Thickness (mm)	Tunability	Transparent
[16]		7–18	93%	0.07\3	Bandwidth	Yes
[18]		11.5–16.5	35%	0.06\1.19	Frequency	No
[19]		11–14.5	27%	0.086\2.4	Frequency	Yes
[23]		10–12	18.1%	0.093\2.8	Absorptivity	No
[24]		22.2–38	66.7%	0.21\2.4	Bandwidth	No
[27]		1.9–13.8	151.6%	0.127\20	N. A.	No
[28]		4.95–38.8	155%	0.417\25	Absorptivity	Yes
Ours	1#	6.8–14	69.2%	0.187\8.25	Absorptivity	Yes
	2#	5.28–39.52	152.8%	0.167\9.5	Absorptivity	Yes

[1] λ_L is the free-space wavelength at the lower frequency of the absorption band.

In [27], a three-dimensional design with integrated resistors is utilized to present an ultra-broadband microwave absorber. This absorber has a fractional bandwidth of 151.6% and a relative thickness of $0.127\lambda_L$. However, it lacks transparency and tunability. Recently, a transparent origami metamaterial absorber has been designed [28]. It offers a bandwidth of 155% and modulated absorptivity. However, its thickness is much greater at $0.417\lambda_L$ than ours. Furthermore, the mechanical tuning method employed in this design has a significantly slower tuning speed than the voltage tuning method. The approach employed in our study is better suited for applications that require both optical transparency and fast broadband reflection modulation.

4. CONCLUSION

In summary, we have successfully developed and validated a microwave absorber that can adjust its absorptivity. This absorber utilizes a hybrid structure composed of Graphene-ITO-PVC layers. The entire structure demonstrates impressive light transmission properties, due to the high optical transmittance of graphene, ITO, and PVC substrate. Moreover, this design allows for a bandwidth of 61.1% with absorption levels exceeding 90%. It also enables dynamic control of reflection within a wide range (-10.5 dB to -4 dB) by adjusting the bias voltage between 0 V and 5 V. By introducing an additional ITO layer with a different impedance between GSS and ITO ground, we can achieve an ultra-broadband absorber that covers a range of

5.28–39.52 GHz, with a fractional bandwidth of 152.8%. This exceptional performance is attributed to the dispersionless resistance of graphene and ITO in microwaves, as well as the nonpatterned configuration. The concept of designing a dynamically adjustable absorber or reflector, combined with its outstanding optical transparency, opens up possibilities for utilizing wave-absorbing materials in various scenarios and provides valuable insights for future advancements in intelligent wireless devices.

ACKNOWLEDGEMENT

This paper is supported by the Natural Science Foundation of Zhejiang Province under Grant LY22F010001, the Natural Science Foundation of Ningbo (2022J098), and the Fundamental Research Funds for the Provincial Universities of Zhejiang.

REFERENCES

[1] Ionut, N., "Electromagnetic pollution in urban areas," in *2014 International Conference and Exposition on Electrical and Power Engineering (EPE)*, 565–570, Iasi, Romania, Oct. 2014.

[2] Bandara, P. and D. O. Carpenter, "Planetary electromagnetic pollution: It is time to assess its impact," *The Lancet Planetary Health*, Vol. 2, No. 12, e512–e514, Dec. 2018.

[3] Zhong, S., W. Jiang, P. Xu, T. Liu, J. Huang, and Y. Ma, "A radar-infrared bi-stealth structure based on metasurfaces," *Applied Physics Letters*, Vol. 110, No. 6, 063502, Feb. 2017.

[4] Takizawa, K. and O. Hashimoto, "Transparent wave absorber using resistive thin film at V-band frequency," *IEEE Transactions on Microwave Theory and Techniques*, Vol. 47, No. 7, 1137–1141, Jul. 1999.

[5] Hanazawa, M., O. Hashimoto, and K. Wada, "An X-band transparent wave absorber using an ITO resistive-film for oblique incident wave," in *2000 30th European Microwave Conference*, 1–4, Paris, France, Oct. 2000.

[6] Tian, S.-C., H. Xue, and L. Li, "An broadband transparent metamaterial absorber using an ITO resistive-film," in *2018 International Workshop on Antenna Technology (iWAT)*, 1–3, Nanjing, China, Mar. 2018.

[7] Bychanok, D., G. Gorokhov, D. Meisak, P. Kuzhir, S. A. Maksimenko, Y. Wang, Z. Han, X. Gao, and H. Yue, "Design of carbon nanotube-based broadband radar absorber for Ka-band frequency range," *Progress In Electromagnetics Research M*, Vol. 53, 9–16, 2017.

[8] Bayrakdar, H., "Electromagnetic propagation and absorbing property of ferrite-polymer nanocomposite structure," *Progress In Electromagnetics Research M*, Vol. 25, 269–281, 2012.

[9] Du Toit, L. J., "The design of Jauman absorbers," *IEEE Antennas and Propagation Magazine*, Vol. 36, No. 6, 17–25, Dec. 1994.

[10] Zhang, C., Q. Cheng, J. Yang, J. Zhao, and T. J. Cui, "Broadband metamaterial for optical transparency and microwave absorption," *Applied Physics Letters*, Vol. 110, No. 14, 143511, Apr. 2017.

[11] Meng, F., H. Jiang, X. Shan, L. Zhou, B. Chen, and W. Yang, "An optically transparent broadband high-efficiency microwave absorber using standing-up circular split rings," in *2021 International Conference on Microwave and Millimeter Wave Technology (ICMMT)*, 1–3, Nanjing, China, May 2021.

[12] Chaudhary, K., G. Singh, J. Ramkumar, S. A. Ramakrishna, K. V. Srivastava, and P. C. Ramamurthy, "Optically transparent protective coating for ITO-coated PET-based microwave metamaterial absorbers," *IEEE Transactions on Components, Packaging and Manufacturing Technology*, Vol. 10, No. 3, 378–388, Mar. 2020.

[13] Nilsson, J., A. H. C. Neto, F. Guinea, and N. M. R. Peres, "Electronic properties of graphene multilayers," *Physical Review Letters*, Vol. 97, No. 26, 266801, Dec. 2006.

[14] Hanson, G. W., "Dyadic Green's functions and guided surface waves for a surface conductivity model of graphene," *Journal of Applied Physics*, Vol. 103, No. 6, 064302, Mar. 2008.

[15] Balci, O., E. O. Polat, N. Kakenov, and C. Kocabas, "Graphene-enabled electrically switchable radar-absorbing surfaces," *Nature Communications*, Vol. 6, No. 1, 6628, May 2015.

[16] Zhang, J., Z. Li, L. Shao, and W. Zhu, "Dynamical absorption manipulation in a graphene-based optically transparent and flexible metasurface," *Carbon*, Vol. 176, 374–382, 2021.

[17] Xiong, H., Y.-N. Jiang, C. Yang, and X.-P. Zeng, "Frequency-tunable terahertz absorber with wire-based metamaterial and graphene," *Journal of Physics D: Applied Physics*, Vol. 51, No. 1, 015102, Jan. 2018.

[18] Geng, M.-Y., Z.-G. Liu, W.-J. Wu, H. Chen, B. Wu, and W.-B. Lu, "A dynamically tunable microwave absorber based on graphene," *IEEE Transactions on Antennas and Propagation*, Vol. 68, No. 6, 4706–4713, Jun. 2020.

[19] Zhong, S., Y. Zhang, and Y. Ma, "Optically transparent frequency-tunable microwave absorber based on patterned graphene-ITO structure," *IEEE Transactions on Antennas and Propagation*, Vol. 70, No. 10, 9959–9964, 2022.

[20] Xue, Z., S. Zhong, X. Wang, and Y. Ma, "Angularly tunable perfect absorption in graphene-mushroom hybrid structure for all angles," *Applied Physics Letters*, Vol. 118, No. 16, 161103, Apr. 2021.

[21] Xue, Z., S. Zhong, and Y. Ma, "Graphene-FSS hybrid absorptive structure with amplitude/frequency dual-modulated passband," *IEEE Antennas and Wireless Propagation Letters*, Vol. 20, No. 9, 1711–1715, Sep. 2021.

[22] Zhang, J., X. Wei, M. Premaratne, and W. Zhu, "Experimental demonstration of an electrically tunable broadband coherent perfect absorber based on a graphene-electrolyte-graphene sandwich structure," *Photonics Research*, Vol. 7, No. 8, 868–874, Aug. 2019.

[23] Zhang, J., Z. Liu, W. Lu, H. Chen, B. Wu, and Q. Liu, "A low profile tunable microwave absorber based on graphene sandwich structure and high impedance surface," *International Journal of RF and Microwave Computer-Aided Engineering*, Vol. 30, No. 2, e22022, 2020.

[24] Feng, J. L., L.-S. Wu, and J.-F. Mao, "Switchable broadband/narrowband absorber based on a hybrid metasurface of graphene and metal structures," *Optics Express*, Vol. 31, No. 8, 12 220–12 231, 2023.

[25] Yi, D., X.-C. Wei, and Y.-L. Xu, "Transparent microwave absorber based on patterned graphene: Design, measurement, and enhancement," *IEEE Transactions on Nanotechnology*, Vol. 16, No. 3, 484–490, May 2017.

[26] Pozar, D. M., *Microwave Engineering*, 4th ed., Wiley, Hoboken, NJ, USA, 2012.

[27] Luo, G. Q., W. Yu, Y. Yu, X. H. Zhang, and Z. Shen, "A three-dimensional design of ultra-wideband microwave absorbers," *IEEE Transactions on Microwave Theory and Techniques*, Vol. 68, No. 10, 4206–4215, Oct. 2020.

[28] Song, Z., J.-F. Zhu, X. Wang, R. Zhang, P. Min, W. Cao, Y. He, J. Han, T. Wang, J. Zhu, L. Wu, and C.-W. Qiu, "Origami metamaterials for ultra-wideband and large-depth reflection modulation," *Nature Communications*, Vol. 15, No. 1, 3181, Apr. 2024.